Decoupling of Apoptosis from Activation of the ER Stress Response by the *Drosophila* Metallopeptidase *superdeath*

Rebecca A. S. Palu,[1] Hans M. Dalton, and Clement Y. Chow[2]
Department of Human Genetics, University of Utah School of Medicine, 15 N 2030 E Salt Lake City, Utah 84112
ORCID IDs: 0000-0001-9444-8815 (R.A.S.P.); 0000-0002-3104-7923 (C.Y.C.)

ABSTRACT Endoplasmic reticulum (ER) stress-induced apoptosis is a primary cause and modifier of degeneration in a number of genetic disorders. Understanding how genetic variation influences the ER stress response and subsequent activation of apoptosis could improve individualized therapies and predictions of outcomes for patients. In this study, we find that the uncharacterized, membrane-bound metallopeptidase *CG14516* in *Drosophila melanogaster*, which we rename as *SUPpressor of ER stress-induced DEATH* (*superdeath*), plays a role in modifying ER stress-induced apoptosis. We demonstrate that loss of *superdeath* reduces apoptosis and degeneration in the $Rh1^{G69D}$ model of ER stress through the JNK signaling cascade. This effect on apoptosis occurs without altering the activation of the unfolded protein response (IRE1 and PERK), suggesting that the beneficial prosurvival effects of this response are intact. Furthermore, we show that *superdeath* functions epistatically upstream of *CDK5*—a known JNK-activated proapoptotic factor in this model of ER stress. We demonstrate that *superdeath* is not only a modifier of this particular model, but affects the general tolerance to ER stress, including ER stress-induced apoptosis. Finally, we present evidence of Superdeath localization to the ER membrane. While similar in sequence to a number of human metallopeptidases found in the plasma membrane and ER membrane, its localization suggests that *superdeath* is orthologous to *ERAP1/2* in humans. Together, this study provides evidence that *superdeath* is a link between stress in the ER and activation of cytosolic apoptotic pathways.

KEYWORDS ER stress; apoptosis; metallopeptidase; modifier genes

ENDOPLASMIC reticulum (ER) stress-induced apoptosis is a primary or contributing cause of degeneration in a wide variety of diseases, such as type 2 diabetes and Alzheimer's disease (Yilmaz 2017; Alicka and Marycz 2018; Kurtishi *et al.* 2018). Reducing stress-induced apoptosis could be the key to slowing the progression of these diseases, and indeed a major focus of therapeutic development is to identify compounds that can inhibit apoptosis. Therapeutics that target cell death without impacting the beneficial survival pathways activated by the ER stress response are essential in the treatment of degenerative diseases.

doi: https://doi.org/10.1534/genetics.119.303004
Manuscript received July 26, 2019; accepted for publication February 9, 2020; published Early Online February 11, 2020.
Supplemental material available at figshare: https://doi.org/10.6084/m9.figshare.11401827
[1]Current address: Biology Department, Purdue University-Fort Wayne, Fort Wayne, IN 46805.
[2]Corresponding author: Eccles Institute of Human Genetics, 15 N 2030 E, Room 5200, Salt Lake City, UT 84112. E-mail: cchow@genetics.utah.edu

ER stress occurs when protein folding is disrupted, leading to the accumulation of misfolded proteins in the ER. ER stress activates the Unfolded Protein Response (UPR)—a massive transcriptional response that, if successful, will return the ER and cell to homeostasis (Schröder and Kaufman 2005). This response is regulated by three sensors that are located in the ER membrane: IRE1, PERK, and ATF6 (Sano and Reed 2013). Upon sensing misfolded proteins, the IRE1 endonuclease domain is activated, allowing it to noncanonically splice the mRNA for the transcription factor *Xbp1*. Once spliced, *Xbp1* is translated and translocates to the nucleus, activating expression of UPR target genes (Cox and Walter 1996; Sidrauski and Walter 1997). IRE1 also degrades a number of ER-targeted transcripts under ER stress conditions (Regulated IRE1 Dependent mRNA Decay or RIDD) (Hollien and Weissman 2006; Hollien *et al.* 2009; Sano and Reed 2013). Upon ER stress, PERK phosphorylates the translation initiation factor eIF2α. This greatly reduces translation of mRNA transcripts with the canonical transcription initiation mechanism, while allowing

increased translation of specific stress-regulated transcripts such as the transcription factor ATF4 (Sano and Reed 2013). Finally, under ER stress, ATF6 is trafficked to the Golgi, where it is processed, releasing the cytoplasmic domain to act as a transcription factor (Sano and Reed 2013). Under conditions of chronic or extreme stress, the UPR may eventually induce apoptosis (Sano and Reed 2013). In *Drosophila*, this is primarily through the activation of the Jun Kinase (JNK) signaling cascade downstream of the apoptotic regulator CDK5 (Kang *et al.* 2012; Sano and Reed 2013). The mechanism through which CDK5 is activated by ER stress and the UPR is unknown.

The ER stress response is strongly influenced by genetic variation (Dombroski *et al.* 2010; Chow *et al.* 2013, 2015, 2016). In a previous study, we modeled the impact of genetic variation on the ER stress response by overexpressing mutant rhodopsin ($Rh1^{G69D}$) in the developing *Drosophila* eye (Chow *et al.* 2016). We crossed this model into the ~200 genetic backgrounds of the *Drosophila* Genetic Reference Panel (DGRP) (Mackay *et al.* 2012; Chow *et al.* 2016). We measured retinal degeneration and performed a genome-wide association analysis to identify modifier variation that is associated with differences in degeneration. We generated a list of 84 conserved candidate modifier genes, ~50% of which have known roles in apoptotic pathways and/or the ER stress response (Chow *et al.* 2016). By characterizing these modifiers, we can learn more about the pathogenesis and progression of ER stress-related diseases.

Here, we report a novel function for one of these modifiers, the *Drosophila* metallopeptidase *CG14516*, which we rename *SUPpressor of ER stress-induced DEATH* (*superdeath*). We demonstrate that, in this $Rh1^{G69D}$ model of ER stress, loss of *superdeath* results in partial rescue of degeneration. This reduced degeneration is accompanied by reduced apoptosis and JNK signaling. This is in the absence of any detectable changes in activation of the ER stress sensors IRE1 or PERK, suggesting that *superdeath* lies downstream of the UPR in the activation of apoptosis. Epistasis experiments indicate that *superdeath* lies genetically upstream of *CDK5*, and that the changes observed in degeneration are possibly due to reduced activation of CDK5. While *superdeath* is orthologous to a number of mammalian metallopeptidases, we show that Superdeath protein can localize to the ER, suggesting that it is functionally related to the ER-associated proteases 1 and 2 (ERAP1 and ERAP2) (Haroon and Inman 2010). Our results indicate that inhibition of Superdeath/ERAP1/ERAP2 would reduce apoptosis levels under conditions of ER stress, while retaining the beneficial effects of UPR activation, making it a valuable target for therapeutic development.

Materials and Methods

Fly stocks and maintenance

Flies were raised at room temperature on standard diet based on the Bloomington Stock Center standard medium with malt. The strain containing *GMR-GAL4* and $UAS\text{-}Rh1^{G69D}$ on the second chromosome ($GMR > Rh1^{G69D}$) has been described previously (Chow *et al.* 2016; Palu and Chow 2018). The following strains are from the Bloomington Stock Center: *MS1096-GAL4* (8696), *UAS-superdeath* RNAi (42947), a second *UAS-superdeath* RNAi (35802), control *attP40* (36304), control *attP2* (36303), *superdeath-GFP* (64447). The *UAS-CDK5* RNAi (104491), the third UAS-superdeath RNAi (108616), and the control attP (60100) lines are from the Vienna *Drosophila* Resource Center. The *puc-LacZ* enhancer trap is available from Kyoto (109029). The strains containing the *UAS-Xbp1-EGFP* transgenes were a gift from Don Ryoo (NYU).

Eye/wing imaging

For eye and wing images, adult females were collected under CO_2 anesthesia, aged to 2–7 days, then flash frozen on dry ice. Eyes were imaged at 3× magnification using a Leica EC3 camera. Wings were dissected away from the body, then imaged at 4.5× magnification using the same camera. Eye and wing area were measured in ImageJ as previously described (Chow *et al.* 2016).

Immunohistochemistry

Eye discs and salivary glands were dissected from wandering L3 larvae in cold 1× phosphate-buffered saline (PBS), then immediately transferred to cold 4% paraformaldehyde (PFA) on ice. S2 cells were treated while adhered to sterile plastic coverslips. Samples were fixed in 4% PFA for 15–20 min, then washed in 1× PAT (1× PBS with 0.1% TritonX100) prior to blocking with 5% normal donkey serum. Samples were stained with primary antibodies for rhodopsin (1:50; #4C5 Developmental Studies Hybridoma Bank), green fluorescent protein (GFP) (1:2000; #A6455 Thermo-Fisher, 1:100; #M048-3 MBL), LacZ (1:20-1:50; #40-1a DSHB), Calnexin 99A (1:50; #cnx99A 6-2-1 DSHB), Golgin-84 (1:50; #golgin-84 12-1 DSHB), Lamp1 (1:100; # ab30687 Abcam), and V5 (1:500; #13202S Cell Signaling, and 1:250; #R960-25 Thermo-Fisher). Apoptosi was monitored using the ApopTag Red *In Situ* Apoptosis Detection Kit (#S7165 Millipore). Samples were mounted in Slowfade Diamond Antifade Mountant (#S36967 Thermo-Fisher) and imaged with an Olympus FV1000 confocal microscope or a Nikon A1 confocal microscope.

Western blots

Protein was isolated from 10 wandering L3 larvae brain-imaginal disc complexes or from S2 cells, and homogenized in 1× Laemmli/radioimmunoprecipitation assay (RIPA) buffer containing 1× protease inhibitors (Roche cOmplete Mini EDTA-free protease inhibitor tablets) as well as the phosphatase inhibitors Calyculin A and okadaic acid. Equivalent amounts of protein were resolved by SDS-PAGE (10% acrylamide) and transferred to polyvinylidene fluoride (PVDF) membrane by semi-dry transfer. Membranes were then treated with either 5% bovine serum albumin (BSA)

or 5% milk protein block in 1× Tris Buffered Saline with Tween (TBST) prior to immunoblotting. Blots were probed with antibodies for P-eif2α (1:1000; #32157 abcam), Pan-eif2α (1:500; #26197 abcam), and tubulin (1:2000; #12G10 Developmental Studies Hybridoma Bank). Blots shown are representative of at least three biological replicates, and quantification was performed using ImageJ.

Tunicamycin treatment

Crosses to generate the indicated genotypes were set up on egg caps containing yeast paste. L2 larvae were then treated with either 10 μg/ml Tunicamycin (diluted 1:1000 from a 10 mg/ml stock solution) or 1:1000 DMSO in Schneider's media for 5 hr at room temperature. The larvae were then washed in 1× PBS twice and placed on standard media. Viability was determined by survival to pupation. Survival for each genotype was normalized to the DMSO-treated control condition. Each replicate represents 112–130 larvae per genotype.

S2 cells

DsRNA was generated using the MEGAscript T7 Transcription kit (#AM1334 ThermoFisher), with primers for *EGFP* (F: TTAATACGACTCACTATAGGGAGACCACAAGTTCAGCGTGTCC and R: TTAATACGACTCACTATAGGGAGAGGGGTGTTCT GCTGGTAGTG) and *superdeath* (F: TTAATACGACTCA CTATAGGGAGATCCGGTGGTTAAGGTGTCAAGG and R: TTA ATACGACTCACTATAGGGAGAGCCGGAGTTGACGAACATGG). S2 cells were treated with DsRNA against *EGFP* (as a control) or against *superdeath* at a density of ∼2 × 10^6 cells/ml in a 24-well plate. Cells were incubated with DsRNA for 4–7 days before being split and treated with either 2 mM DTT or DMSO as a control. Cells were treated for 4 hr for *Xbp1* splicing and P-eif2a measurements and for 7.5 hr for *rpr* and *hid* measurements. RNA was isolated from cells using the Direct-zol RNA Miniprep Kit and used to generate cDNA (Protoscript II, NEB). Protein was isolated from cells as described above.

Knockdown of *superdeath* was confirmed using qPCR (primers: F: ATTCGCAGCAGTTTCCACCAC and R: TTCGTGGCGAACTT GAACAGC). *Xbp1* splicing was evaluated from the cDNA using PCR (primers for *Xbp1:* F: TCAGCCAATCCAACGCCAG and R: TGTTGTATACCCTGCGGCAG). The spliced and unspliced bands were separated on a 12% acrylamide gel, and the proportion of these bands quantified using ImageJ software. *rpr* (F: TTGCGGGAGTCACAGTGGAG and R: AATCCTCATTGC GATGGCTTGC) and *hid* (F: TACCTACTACGCGGGCTACACG and R: TGGTACTCGCGCTCATCCTC) levels were analyzed by qPCR. Transcript levels were normalized to *rpl19* (F: AGGTCGG ACTGCTTAGTGACC and R: CGCAAGCTTATCAAGGATGG) and compared between matched DMSO or DTT-treated S2 cells.

Cloning

Superdeath was overexpressed in S2 cells using the TOPO TA Cloning Kit (Thermo-Fisher). The coding sequence for *superdeath* was expressed from the pMT-DEST48 inducible expression vector with a C-terminal V5 tag. S2 cells adhered to sterile glass cover slips were made competent using the Calcium Phosphate Transfection Kit (Thermo-Fisher), and expression of the construct was induced with 500 μM $CuSO_4$ for 66 hr. Cells were then stained for the V5 tag and other subcellular markers to determine Superdeath protein localization as described above.

Statistics

Statistics were calculated using R or Prism software. *P*-values were determined using either one-way or two-way ANOVA for eye size, fluorescence levels, and transcript levels in qPCR. A pairwise T-test was performed for larval tunicamycin treatment. A cutoff of $P = 0.05$ was used for significance.

Reagent and data availability

The authors state that all data necessary for confirming the conclusions presented in the article are represented fully within the article. Strains and stocks are available upon requests. Supplemental material is available at figShare (https://figshare.com/articles/SupplementalFiles_superdeath_pdf/11401827).

Results

A single nucleotide polymorphism in CG14516 is associated with variation in expression and degeneration in the $Rh1^{G69D}$ model of ER stress

In a previous study, we examined the impact of genetic variation on ER stress-induced apoptosis using a model of ER stress in which we overexpressed mutant, misfolding rhodopsin in the developing eye imaginal disc using the *GAL4/UAS* system (*GMR-GAL4 > UAS-*$Rh1^{G69D}$) (Chow *et al.* 2016). We crossed this model of retinal degeneration and ER stress into the *Drosophila* Genetic Reference Panel (DGRP)—a collection of ∼200 wild-derived isogenic strains (Mackay *et al.* 2012). We performed a genome-wide associated analysis to identify candidate modifier genes of ER stress and degeneration (Chow *et al.* 2016). As half of the genome in the F1 flies came from the DGRP parent and the other from the model "donor" strain, all candidate modifiers were identified from dominant interactions. One of these candidate genes is *CG14516*—a previously uncharacterized membrane-bound metallopeptidase. A single nucleotide polymorphism (SNP) in the first intron of *CG14516* is significantly associated with eye size in the $Rh1^{G69D}$ model ($P = 2.24 \times 10^{-5}$, Figure 1A). Strains carrying the major "A" allele have larger, less degenerate eyes (21,922 ± 2279 pixels) compared to those carrying the minor "T" allele (19,863 ± 2873 pixels). We next asked if this SNP is associated with differences in *CG14516* expression levels by mining previously published, publically available RNA-seq expression data from the DGRP (Huang *et al.* 2015). The minor "T" allele is associated with a small, but significant, increase in *CG14516* expression in adult females [9.09 ± 0.24 $\log_2$ (FPKM +1)] compared to the major "A" allele [8.84 ± 0.30 $\log_2$ (FPKM +1), $P = 4.92 \times 10^{-3}$,

Figure 1B] (Huang *et al.* 2015). Importantly, expression levels of *CG14516* in adult females is inversely correlated with eye size in the presence of $Rh1^{G69D}$ ($r = -0.25$, $P = 0.0013$, Figure 1C). These data show that reduced expression of *CG14516* is associated with a decrease in $Rh1^{G69D}$-induced degeneration, suggesting that loss of *CG14516* function should reduce ER stress-induced degeneration. We have therefore named this gene *SUPpressor of ER stress-induced DEATH* (*superdeath*).

Loss of superdeath expression rescues $Rh1^{G69D}$-induced apoptosis and degeneration

To test the impact of *superdeath* expression on $Rh1^{G69D}$-induced degeneration, we expressed an RNAi construct targeting *superdeath* in the presence of the $Rh1^{G69D}$ model of ER stress ($Rh1^{G69D}$/*superdeathi*). As in the original model, we used the *GMR* promoter to turn on expression of $Rh1^{G69D}$, RNAi, and other *UAS*-transgenes early in L3 development (FlyBase Curators 2017). Expression of $Rh1^{G69D}$ begins to immediately activate the UPR. We performed all staining and Western blots on tissues collected at the late, wandering L3 stage, well after the UPR has been initiated. In previous studies using this model (Kang *et al.* 2012; Palu and Chow 2018), the late L3 stage has been successfully monitored for activation of the UPR and associated cell death, while adults exhibit stable, abnormal eye phenotypes upon eclosion. To confirm knockdown levels, ubiquitous expression of the *superdeath* RNAi construct results in a 75% reduction in *superdeath* expression (0.278 ± 0.072 relative to controls at 1.00 ± 0.16, $P = 1.77 \times 10^{-4}$, Supplemental Material, Figure S1A).

We found that, in the absence of *superdeath*, eye size is significantly increased ($15{,}299 \pm 1658$ pixels) compared to a control that is only expressing $Rh1^{G69D}$ ($Rh1^{G69D}$/control) ($11{,}942 \pm 473$ pixels, $P = 8.15 \times 10^{-6}$, Figure 2A). This increase was recapitulated using two additional RNAi lines (Figure S1, B and C), indicating that the increase in eye size is indeed due to a loss of *superdeath* expression. We observe a slight increase in eye size when we reduce expression of *superdeath* in wild-type eyes compared to controls, but no qualitative difference ($28{,}867 \pm 1566$ pixels *vs.* $25{,}968 \pm 1026$ pixels in controls, $P = 1.16 \times 10^{-4}$, Figure 2B). While this may indicate an impact on apoptosis under control conditions, the proportional difference is too small to detect dramatic differences. Indeed, wild-type eye imaginal discs display so little apoptosis at the stage we are observing that we would be unable to measure a reduction in cell death.

In our laboratory, we have validated 25 candidates from the original screen in this way. Loss of 7 of these genes enhances degeneration, loss of 8 genes enhances degeneration, and loss of 10 genes has no effect (Chow *et al.* 2016; Palu and Chow 2018; data not published). The varied impact of RNAi knockdown of candidate genes suggests that the phenotypes we observe are unlikely to be a result of either of GAL4 dilution or nonspecific activation of the RNAi system.

Because reduced degeneration in the $Rh1^{G69D}$ model of ER stress is often accompanied by reduced apoptosis (Kang *et al.* 2012; Palu and Chow 2018), we measured cell death in the eye imaginal disc, a developmental structure that will eventually become the adult eye. This tissue is also the site of mutant rhodopsin overexpression, and where ER stress and apoptosis are being induced. TUNEL staining indicates that there is reduced apoptosis in the absence of *superdeath* (47 ± 27 cells) compared to $Rh1^{G69D}$/controls (104 ± 21 cells, $P = 0.044$, Figure 2, C and D). Our findings demonstrate that *superdeath* is required for high levels of ER stress-induced apoptosis and subsequent degeneration. The rescue effect observed upon loss of *superdeath* is likely due to this reduced apoptosis.

Because ubiquitous loss of *superdeath* is lethal during pupal stages (see below), we were unable to use null alleles to confirm our tissue-specific RNAi findings. To confirm these in an alternate system, we treated *Drosophila* S2 cells with DsRNA targeting either *superdeath* or *EGFP* as a control. The DsRNA targets a region of *superdeath* independent from that targeted by the RNAi, making it a good validation of the *in vivo* model. Treatment of S2 cells with DsRNA against *superdeath* resulted in 90% reduction in *superdeath* expression (0.102 ± 0.038 relative to controls at 1.00 ± 0.29, $P = 1.9 \times 10^{-5}$, Figure S1D).

S2 cells were then treated with dithiothreitol (DTT) to induce ER stress. DTT disrupts disulfide bond formation, and results in massive protein misfolding, ER stress, and the induction of the UPR (Jämsä *et al.* 1994). The use of a chemical induction method for ER stress allows us to test *superdeath* with an alternate, independent form of ER stress. Additionally, all cells in the culture will be undergoing ER stress. It is easier to detect stress responses in S2 cells than in the *in vivo* model, where the signal is often overwhelmed by the background signal from other, unaffected, cells in the tissue.

We monitored expression of the apoptosis-associated transcripts *reaper* (*rpr*) and *hid* to determine if there is a difference in the induction of apoptosis when *superdeath* expression is reduced in S2 cells; reaper and hid are inhibitor proteins that target the Inhibitor of Apoptosis Proteins (IAPs), enabling caspase activation and the initiation of apoptosis (Hay *et al.* 1995; Kuranaga *et al.* 2002). Their expression is upregulated under most apoptosis-inducing conditions (Shlevkov and Morata 2012; Mollereau and Ma 2014). Additionally, overexpression of both *rpr* and *hid* is sufficient to induce apoptosis (Hay *et al.* 1995; Goyal *et al.* 2000). Their expression is a good read-out of the activation of a variety of apoptotic pathways (Bilak and Su 2009; Shlevkov and Morata 2012; Zhai *et al.* 2012). As expected, treatment of control S2 cells with DTT results in a ~2.25-fold increase in *rpr* expression (2.23 ± 0.33) compared to cells treated with DMSO (1.00 ± 0.09, $P < 10^{-7}$), indicating that a larger percentage of the DTT-treated cells are undergoing cell death (Figure 2E). In contrast, S2 cells lacking expression of *superdeath* that are treated with DTT display an ~1.5-fold increase in *rpr* expression (1.47 ± 0.07) as compared to DMSO-treated cells (1.00 ± 0.11, $P = 1.2 \times 10^{-3}$, Figure 2E). This response is significantly weaker than that seen in

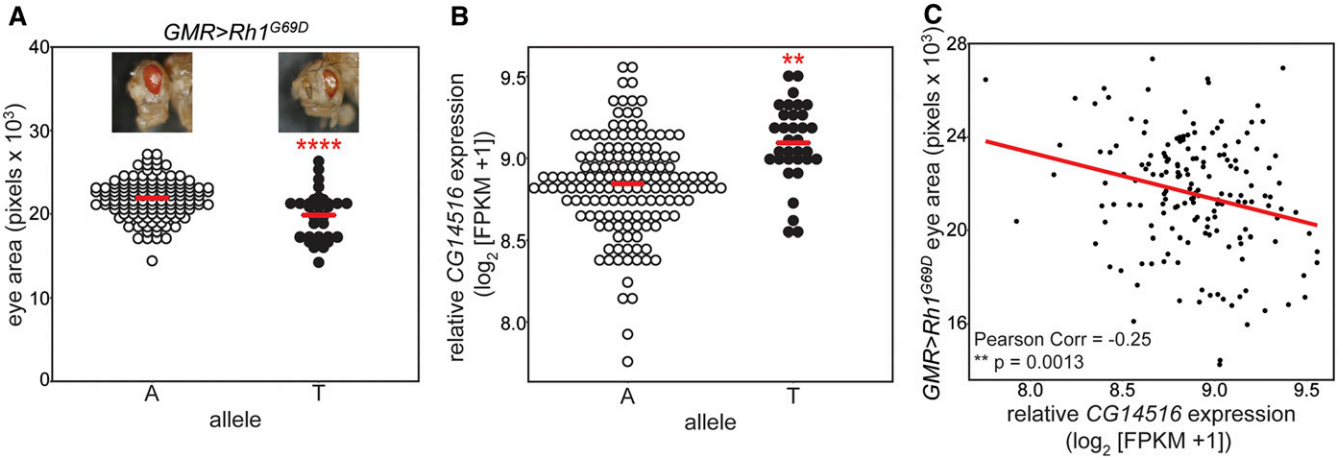

Figure 1 A single nucleotide polymorphism (SNP) in *CG14516* is associated with changes in expression and degeneration. Variation in sequence and expression of the *Drosophila melanogaster* gene *CG14516* is associated with eye size in the $Rh1^{G69D}$ model of ER stress. (A) The 3R:24966022 SNP in *CG14516* (BDGP R5/dm3) is associated with $Rh1^{G69D}$-induced degeneration. $Rh1^{G69D}$ DGRP eye size is plotted by allele identity. Strains carrying the minor "T" allele (19,863 ± 2873 pixels, $N = 32$) have significantly smaller eyes than those carrying the major "A" allele (21,922 ± 2279 pixels, $N = 136$). Representative strains are shown. (B) Expression of *CG14516* in strains carrying either the "A" or the "T" allele was determined from previously published, publically available RNA sequencing data in adult females (Huang *et al.* 2015). *CG14516* levels was significantly increased in strains carrying the minor "T" allele (9.09 ± 0.24 units, $N = 33$) as compared to those carrying the major "A" allele (8.84 ± 0.30 units, $N = 147$). (C) Eye size in the $Rh1^{G69D}$ DGRP strains is inversely correlated with *CG14516* expression levels in adult females ($r = -0.25$, $N = 167$, $P = 0.0013$). Raw data for (A) and (C) were taken from Chow *et.al*. 2016 and Huang *et.al*. 2015, respectively. Values are average ± SD $^{**}P < 0.005$, $^{****}P < 0.00005$.

control cells ($P = 3.5 \times 10^{-6}$). A similar trend was observed for *hid* expression levels (Figure S2). Treatment of control S2 cells with DTT results in a threefold increase in *hid* expression (2.93 ± 1.98) compared to cells treated with DMSO (1.00 ± 0.284, $P = 0.020$). In contrast, S2 cells lacking expression of *superdeath* that are treated with DTT do not display a significant increase in *hid* expression (1.74 ± 0.75) compared to cells treated with DMSO (1.00 ± 0.40, $P = 0.250$). These results support a role for *superdeath* in apoptosis activation.

superdeath regulates JNK signaling independently of UPR activation

In *Drosophila* models of ER stress, and specifically in this model, apoptosis is initiated through activation of the JNK signaling cascade (Kang *et al.* 2012; Zhang *et al.* 2016). To determine if JNK signaling is disrupted upon loss of Superdeath activity, we monitored the expression of a known Jun target gene, *puckered* (*puc*). We used an allele of *puc* wherein the coding sequence has been replaced by the coding sequence for *LacZ*, such that *LacZ* expression is driven by the promotor and regulatory sequences that normally govern *puc* expression (Kanda and Miura 2004). LacZ levels serve as a direct readout for binding of the *puc* promotor by the Jun transcription factor. As expected, we detected high expression of LacZ in the $Rh1^{G69D}$/control eye imaginal discs (1.00 ± 0.39, Figure 2F). This expression is significantly reduced in the absence of *superdeath* (0.367 ± 0.082 relative to controls, $P = 0.043$, Figure 2, F and G). Our findings support a model of reduced signaling through the JNK cascade, which ultimately results in reduced apoptosis.

Loss of superdeath does not impact the activation of UPR signaling pathways

We hypothesized that the reduction in apoptosis and JNK signaling observed in the absence of *superdeath* might be caused by reduced activation of the UPR. We therefore monitored the activation of two of the UPR sensors: IRE1 and PERK. We have chosen to focus on these two pathways as there are no validated targets of ATF6 in *Drosophila* that are independent from other ER stress pathways. IRE1 is the most conserved of the ER stress sensors. When activated by the accumulation of misfolded proteins, the RNAse domain of IRE1 is responsible for the noncanonical splicing of the mRNA for the transcription factor *Xbp1* (Sidrauski and Walter 1997; Sano and Reed 2013). The spliced isoform of *Xbp1* is then translated and travels to the nucleus, where it activates expression of UPR target genes. We monitored IRE1 activity in the eye imaginal disc using an *Xbp1* transgene where the 3′ end of the transcript has been replaced with the coding sequence for *EGFP*, such that EGFP is expressed only under conditions that induce IRE1 activity and *Xbp1* splicing (Ryoo *et al.* 2007, 2013; Sone *et al.* 2013; Huang *et al.* 2017). IRE1 activity was measured by staining for EGFP in eye imaginal discs dissected from $Rh1^{G69D}$/control and $Rh1^{G69D}$/*superdeathi* flies. We also monitored $Rh1^{G69D}$ levels using an antibody against rhodopsin to determine if there are differences in the amount of misfolded protein being expressed. We detected no significant differences in either EGFP (0.905 ± 0.057 relative to 1.00 ± 0.25 in controls) or rhodopsin levels (0.899 ± 0.071 relative to 1.00 ± 0.10 in controls, Figure 3, A–C). Similarly, there was no significant difference in *Xbp1* splicing after exposure to DTT in S2 cells

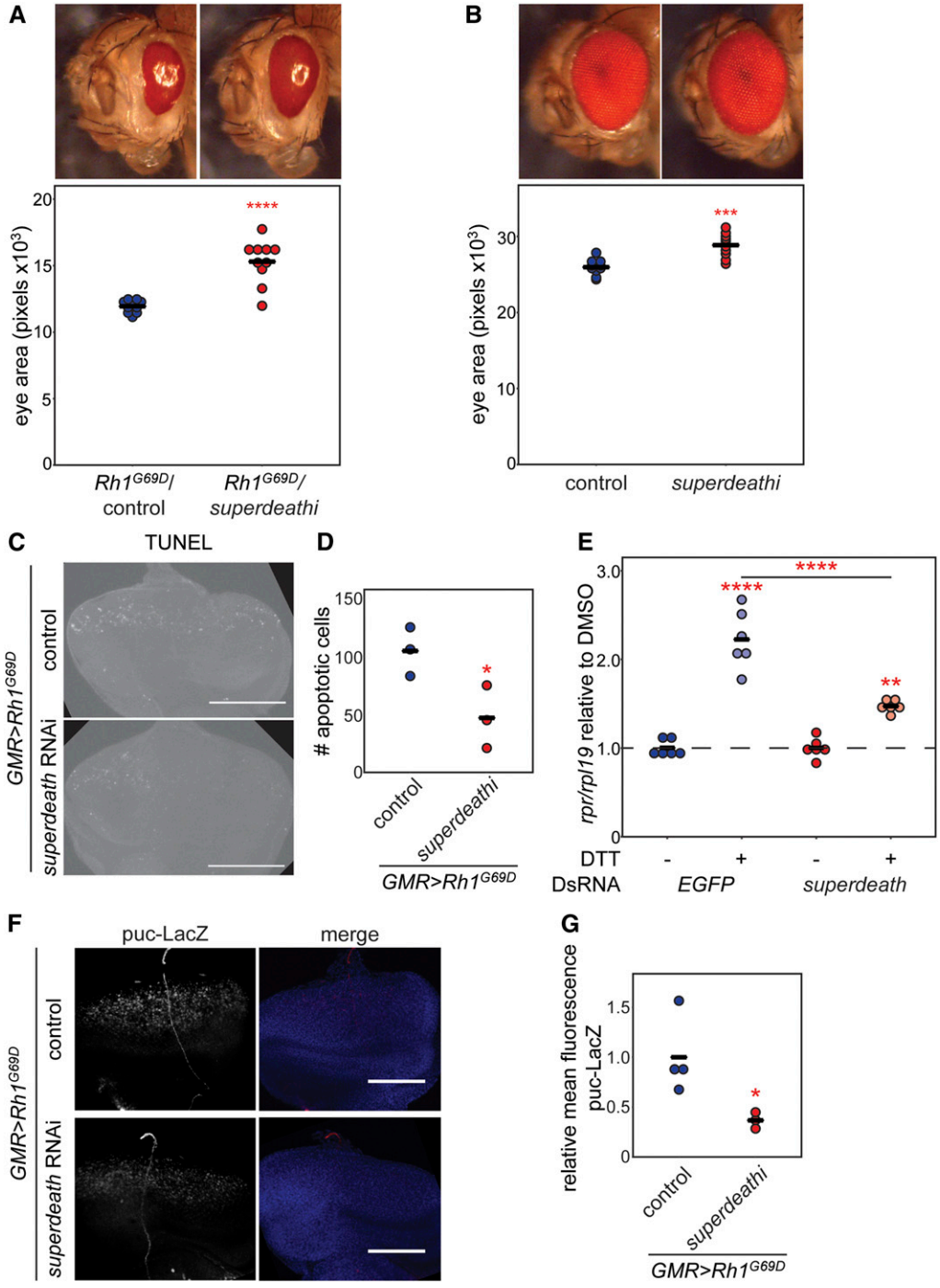

Figure 2 Loss of *superdeath* reduces ER stress-associated apoptosis. Reducing expression of *superdeath* reduces apoptosis and degeneration in models of ER stress. (A) Degeneration caused by overexpression of $Rh1^{G69D}$ is partially rescued by RNAi-mediated knockdown of *superdeath* expression (15,299 ± 1658 pixels, N = 10 in $Rh1^{G69D}$/*superdeathi* flies as compared to 11,942 ± 473 pixels, N = 10 in $Rh1^{G69D}$/controls). (B). Eye size also showed a small increase when the *superdeath* RNAi construct was expressed in a wild-type background (28,867 ± 1566 pixels, N = 10) as compared to controls (25,968 ± 1026 pixels, N = 10), but no qualitative differences were observed. (C). $Rh1^{G69D}$/*superdeathi* eye imaginal discs display reduced apoptosis compared to $Rh1^{G69D}$/controls as measured by TUNEL staining. (D) S2 cells treated with DsRNA against *EGFP* showed increased expression of the apoptotic gene *rpr* after 7.5 hr of DTT exposure (2.23 ± 0.33, N = 6) as compared to DMSO-treated control cells (1.00 ± 0.09, N = 6). Activation of *rpr* expression was significantly reduced in S2 cells that were treated with DsRNA against *superdeath* (1.47 ± 0.07, N = 6 in DTT-treated cells compared to 1.00 ± 0.11, N = 6 with DMSO). (E) Activation of JNK signaling was reduced in $Rh1^{G69D}$/*superdeathi* eye imaginal discs compared to $Rh1^{G69D}$/controls as determined by expression of *puc-LacZ*. (F) When quantified, LacZ levels were significantly lower in $Rh1^{G69D}$/*superdeathi* eye discs (0.367 ± 0.082, N = 3) as compared to $Rh1^{G69D}$/controls (1.00 ± 0.39, N = 4). Values are average ± SD. Bar = 0.1mm. *P < 0.05, **P < 0.005, ****P < 0.00005.

treated with DsRNA targeting *EGFP* or *superdeath* (Figure 3D). These results collectively demonstrate that loss of *superdeath* does not influence IRE1 activation in response to ER stress.

The second major sensor of the UPR is the kinase PERK, which, upon activation by the accumulation of misfolded proteins, phosphorylates the translation initiation factor eif2a. This modification reduces the efficiency of canonical translation initiation while allowing for increased translation of select UPR regulators such as the transcription factor ATF4 (Sano and Reed 2013). To assess PERK activity, we monitored eif2α phosphorylation by Western blot of samples isolated from brain-imaginal disc complexes of $Rh1^{G69D}$/*superdeathi* and $Rh1^{G69D}$/control larvae. We detected no significant differences in P-eif2α accumulation in these samples relative to Pan-eif2α (1.34 ± 0.81 compared to 1.06 ± 0.54 in controls, P = 0.651), suggesting that PERK activity is also unaffected by reduced expression of *superdeath* (Figure 3, E and F). Phosphorylation of eif2α after DTT treatment is also similar between cells treated with

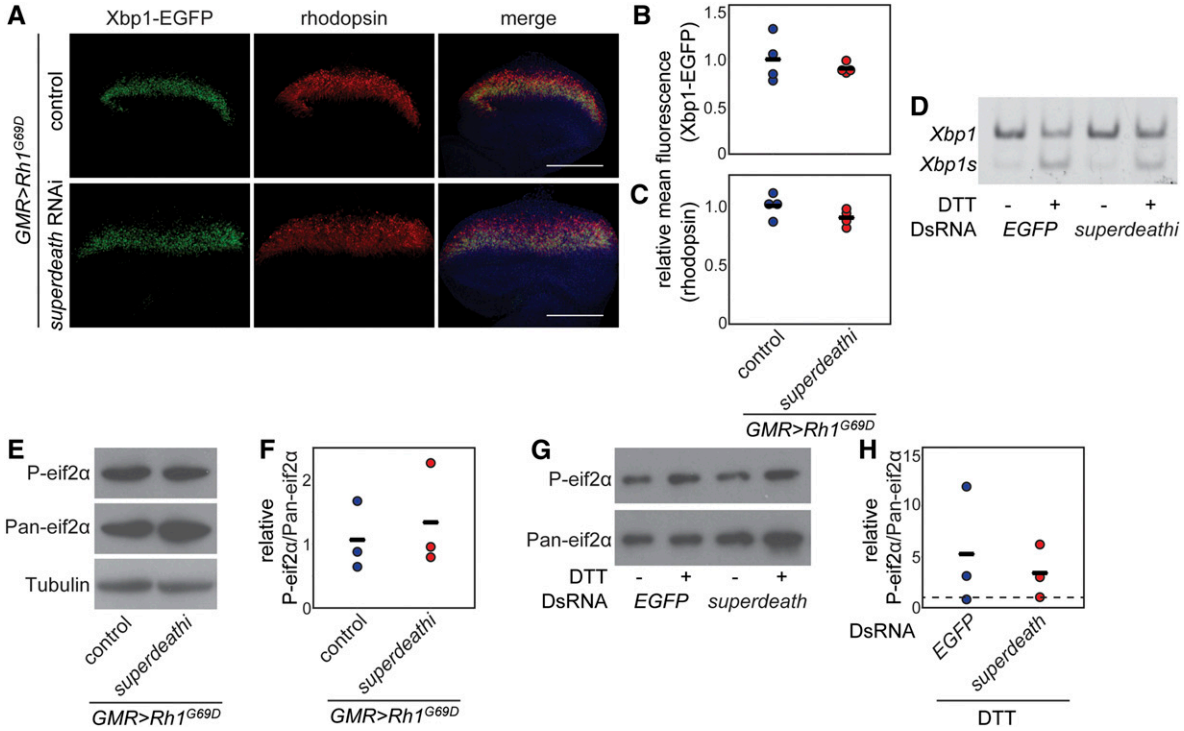

Figure 3 Loss of *superdeath* does not alter IRE1 or PERK activation. Activation of the UPR is not altered by loss of *superdeath* in models of ER stress. (A) *Rh1*^{G69D}*/superdeathi* eye discs do not display altered expression of Xbp1-EGFP or rhodopsin as compared to *Rh1*^{G69D}/controls. Eye discs were dissected from wandering L3 larvae expressing *Rh1*^{G69D} and *UAS-Xbp1-EGFP*, stained for rhodopsin and GFP and counterstained with 4′,6-diamidino-2-pheneylindole (DAPI). (B) Loss of *superdeath* does not significantly alter Xbp1-EGFP expression (0.905 ± 0.057, *N* = 4) compared to *Rh1*^{G69D}/controls (1.00 ± 0.25, *N* = 4). (C) Rhodopsin levels were also not significantly altered (0.899 ± 0.071, *N* = 4 relative to 1.00 ± 0.10, *N* = 4 in controls). (D) DTT treatment increased *Xbp1* splicing in S2 cells compared to control cells treated with DMSO. This increase was similar in S2 cells treated with DsRNA against either *EGFP* or *superdeath*. (E) *Rh1*^{G69D}*/superdeathi* eye discs had similar levels of P-eif2α as compared to *Rh1*^{G69D}/controls. (F) Loss of *superdeath* does not significantly alter the ratio of P-eif2α/Pan-eif2α compared to Rh1^{G69D} controls (1.37 ± 0.81, *N* = 3 relative to 1.06 ± 0.54, *N* = 3). (G) DTT treatment in S2 cells increased levels of P-eif2α compared to the control DMSO treatment. This increase was similar to cells treated with DsRNA against either *EGFP* or *superdeath*. H. Loss of superdeath does not significantly alter the increase in relative P-eIF2α levels seen upon treatment with DTT as compared with control cells (3.42 ± 2.61, *N* = 3 relative to 5.28 ± 5.85, *N* = 3). Relative ratio of P-eIF2α/Pan-eIF2α upon DMSO treatment is indicated by the dotted line (*N* = 3/group). Values are average ± SD. Bar = 0.1 mm.

DsRNA against either *EGFP* or *superdeath* ($P = 0.641$) (Figure 3, G and H).

Collectively, these results indicate that loss of *superdeath* activity does not impact the UPR, and the reduced apoptosis and JNK signaling observed in the absence of *superdeath* is independent of UPR activation or the accumulation of misfolded proteins.

superdeath functions upstream of CDK5 in ER stress-induced apoptosis

superdeath could be regulating general apoptosis signaling or could act more specifically on pathways activated by the UPR. To test if *superdeath* is generally involved in the regulation of cell death, we expressed RNAi targeting *superdeath* in the developing eye imaginal discs of flies overexpressing the cell death initiators *p53* and *rpr*. p53 is primarily activated by the DNA damage response and can initiate apoptosis by transcriptionally activating the IAP inhibitors *rpr*, *grim*, and *hid* (Mollereau and Ma 2014). *rpr* is activated transcriptionally by p53 and the JNK signaling cascade (Kanda and Miura 2004; Shlevkov and Morata 2012; Mollereau and Ma 2014). Overexpression of either of these factors in the eye imaginal disc is sufficient to induce extensive apoptosis and a retinal degenerative phenotype in adult flies in the absence of any additional stressor (Hay *et al.* 1995; Jin *et al.* 2000). We can test the impact of *superdeath* expression on general apoptotic pathways by expressing the RNAi construct targeting *superdeath* in models of *p53* or *rpr* overexpression and evaluating changes in eye degeneration.

We first tested loss of *superdeath* in a model of *p53* overexpression (*p53/superdeathi*) to determine whether general cell death pathways are impacted. We found no difference in eye size between *p53*/control (14,852 ± 1126 pixels) and *p53/superdeathi* flies (15,315 ± 1000 pixels, Figure 4A). We next tested *superdeath* function in a model of *rpr* overexpression (*rpr/superdeathi*) to see if the function of this gene lies upstream or downstream of the transcriptional program that commonly activates apoptosis. As with *p53*, there was no difference in eye size between *rpr*/control (18,953 ± 834 pixels) and *rpr/superdeathi* flies (19,288 ± 664 pixels, Figure 4B). Our findings suggest that *superdeath* functions upstream of the transcriptional program that initiates apoptosis

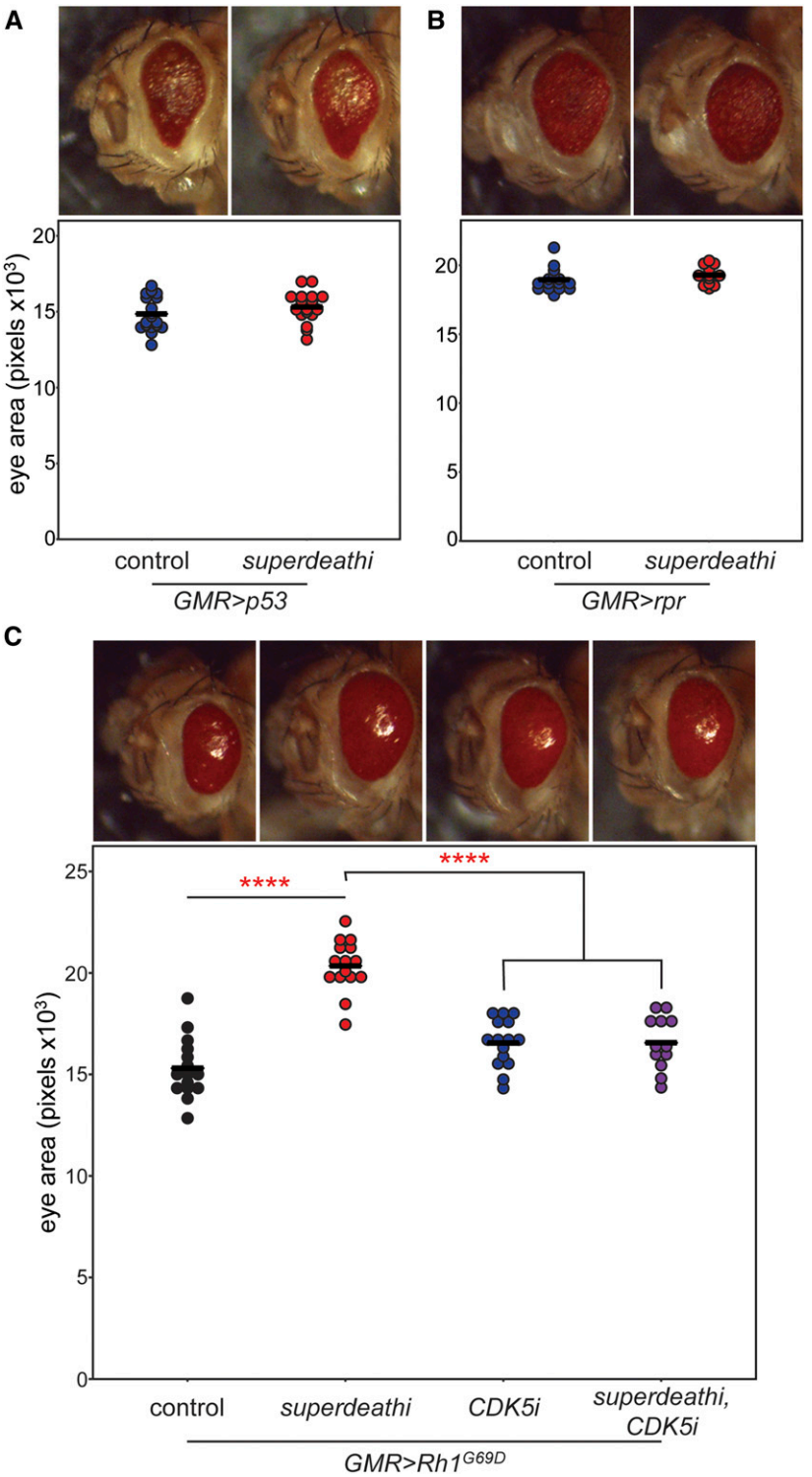

Figure 4 *superdeath* is upstream of *CDK5* in the initiation of ER stress-induced apoptosis. *superdeath* acts specifically in ER stress-associated cell death, upstream of the transcription of apoptotic activators. (A) Degeneration caused by overexpression of *p53* is not altered by RNAi-mediated knockdown of *superdeath* expression (15,315 ± 1000 pixels, N = 18 in *p53*/*superdeathi* flies compared to 14,852 ± 1126 pixels, N = 18 in *p53*/controls). (B) Degeneration caused by overexpression of *rpr* is also unaffected by loss of *superdeath* expression (19,288 ± 664 pixels, N = 13 in *rpr*/*superdeathi* flies compared to 18,953 ± 834 pixels, N = 15 in *rpr*/controls). (C) Degeneration caused by overexpression of $Rh1^{G69D}$ in the absence of both *CDK5* and *superdeath* (16,560 ± 1320 pixels, N = 12) does not significantly differ from degeneration in the absence of *CDK5* alone (16,552 ± 1179 pixels, N = 15). Degeneration is qualitatively improved by RNAi-mediated knockdown of *CDK5* expression although eye size is not significantly increased compared to $Rh1^{G69D}$/controls (15,307 ± 1482 pixels, N = 15). This is in contrast to the significant increase in eye size when *superdeath* expression is reduced (20,346 ± 1292 pixels, N = 15). Values are average ± SD. ****$P < 0.00005$.

and in a pathway that is specific to ER stress. These data also indicate that *superdeath* does not ubiquitously modify general apoptotic pathways.

Activation of JNK-induced apoptosis in the $Rh1^{G69D}$ model of ER stress is regulated by the ser-thr kinase CDK5. Loss of *CDK5* leads to reduced activation of apoptosis without altering the activation of the UPR (Kang *et al.* 2012). These molecular changes are accompanied by qualitative improvements in eye size and pigmentation (Kang *et al.* 2012; Chow *et al.* 2016). We hypothesized that *superdeath* might function in this pathway. To test this, we expressed RNAi constructs targeting *CDK5* and *superdeath*, individually and concurrently, in the developing eye imaginal discs expressing the misfolded $Rh1^{G69D}$ protein. We monitored degeneration using eye size in adult flies. As expected, loss of *superdeath* ($Rh1^{G69D}$/*superdeathi*) results in a substantial and significant increase in eye

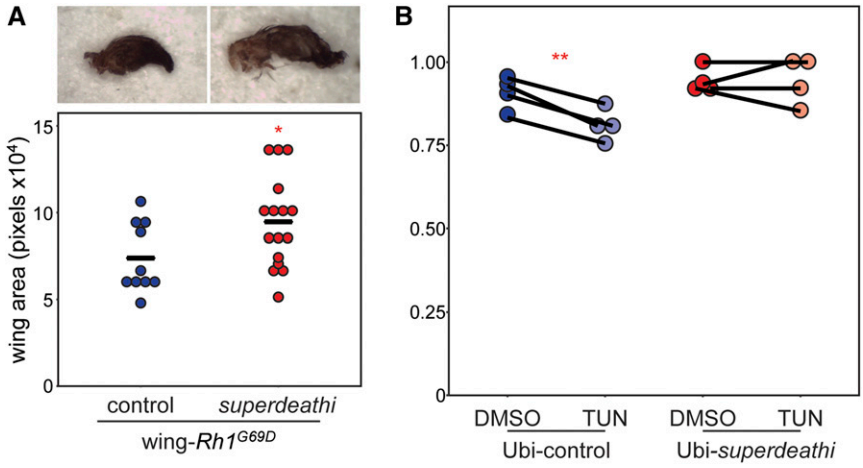

Figure 5 *superdeath* is a general regulator of ER stress-induced cell death. The ER stress response and subsequent apoptosis is subject to regulation by *superdeath* across ER stress conditions. (A) Loss of *superdeath* partially rescues the vestigial wing phenotype caused by expression of $Rh1^{G69D}$ in the wing disc (94,627 ± 26,363 pixels, N = 16 in wing-$Rh1^{G69D}$/*superdeathi vs.* 73,931 ± 19,988 pixels, N = 10 in wing-$Rh1^{G69D}$/controls). (B) Larvae with ubiquitous knockdown of *superdeath* are significantly more resistant to tunicamycin-induced ER stress than control larvae. Four paired experimental replicates are shown, representing a combined total of N = 113 DMSO-treated and N = 130 TUN-treated Ubi-control larvae, and N = 112 DMSO-treated and N = 127 TUN-treated Ubi-*superdeathi* larvae. Values are average ± SD. *P < 0.05, **P < 0.005.

size as compared to the $Rh1^{G69D}$/controls (20,345 ± 1292 pixels *vs.* 15,307 ± 1482 pixels in controls, P < 0.00005, Figure 4C). In line with previous reports (Kang *et al.* 2012; Chow *et al.* 2016), expressing the misfolded $Rh1^{G69D}$ protein and RNAi against *CDK5* ($Rh1^{G69D}$/*CDK5i*) results in a qualitative eye rescue and improvement, but no change in eye size as compared to controls (16,552 ± 1179 pixels, P = 0.060, Figure 4C). Because the phenotype associated with loss of *CDK5* is distinguishable from the phenotype associated with loss of *superdeath*, we can perform an epistasis experiment to determine which of these genes lies downstream of the other. We found that flies simultaneously expressing both RNAi against *CDK5* and *superdeath* ($Rh1^{G69D}$/*CDK5i-superdeathi*) display similar phenotypes to $Rh1^{G69D}$/*CDK5i* flies, with no quantitative improvement in eye size as compared to controls (16,560 ± 1320 pixels, P = 0.081, Figure 4C). We concluded that *superdeath* must operate upstream of *CDK5* to regulate the activation of JNK signaling and apoptosis.

superdeath regulates ER stress-induced apoptosis in multiple tissues

Because CDK5 and JNK signaling occur across different ER stress conditions, we tested whether *superdeath* can act as a modifier across different tissues and methods of ER stress initiation. The wing imaginal disc is a developmental structure that will eventually mature and become the adult wing. Wing imaginal disc expression of a misfolded protein such as $Rh1^{G69D}$ using the *MS1096-GAL4* driver (wing-$Rh1^{G69D}$/conrol) induces ER stress and apoptosis, resulting in a small, degenerate wing that fails to unfold upon eclosion (Figure 5A). Concurrent expression of $Rh1^{G69D}$ and RNAi against *superdeath* (wing-$Rh1^{G69D}$/*superdeathi*) results in partial rescue of the degenerate wing phenotype (Figure 5A), similar to what was observed for the eye. This is also reflected in wing area, which increases from wing-$Rh1^{G69D}$/*superdeathi* (94,627 ± 26,363 pixels) flies compared to wing-$Rh1^{G69D}$/control (73,931 ± 19,988 pixels, P = 0.044, Figure 5A) flies.

To determine whether *superdeath* also responds to diverse mechanisms of initiating ER stress, we ubiquitously expressed RNAi targeting *superdeath* using the *Tub-GAL4* driver (Ubi-*superdeathi*). We then exposed Ubi-*superdeathi* larvae along with controls expressing only *Tub-GAL4* (Ubi-control) to tunicamycin or DMSO for 4 hr. Tunicamycin inhibits N-linked glycosylation in the ER, inducing a massive ER stress response through the UPR (Samali *et al.* 2010). This 5-hr treatment is sufficient to significantly activate the UPR in the larvae, leading to developmental delay and lethality (Huang *et al.* 2015; Kang *et al.* 2015). Because ubiquitous loss of *superdeath* leads to almost complete lethality during pupal stages, we used survival to the pupal stage as our readout for sensitivity to tunicamycin. We found that Ubi-*superdeathi* larvae are significantly more resistant to tunicamycin-induced lethality as compared to Ubi-control larvae (Figure 5B and Table S1). We concluded from these results, and the S2 cell data above, that *superdeath* is generally important for the downstream consequences of ER stress.

Superdeath is localized to the ER

Based on sequence analysis using TMHMM and Scan Prosite tools, Superdeath is hypothesized to contain a single transmembrane domain near the N-terminal of the protein, with the active zinc metalloprotease site localized to the cytoplasm of the cell between amino acids 404 and 413 (Krogh *et al.* 2001; de Castro *et al.* 2006). This active site and the position of the transmembrane domain, are highly conserved when compared to human orthologs. Based on our results described above, we hypothesized that Superdeath could be localized to the ER membrane. Here, among other possibilities, it may be able to sense the activation of ER stress pathways, and activate the cytosolic CDK5-JNK signaling cascade.

To test this, we performed immunofluorescence staining for Superdeath in S2 cells and looked for colocalization with known subcellular markers: Calnexin 99A (ER), Golgin-84 (Golgi), and Lamp1 (lysosome). We induced expression of a transgenic Superdeath tagged with the V5 epitope in S2 cells, and stained for V5 and each subcellular marker. We found

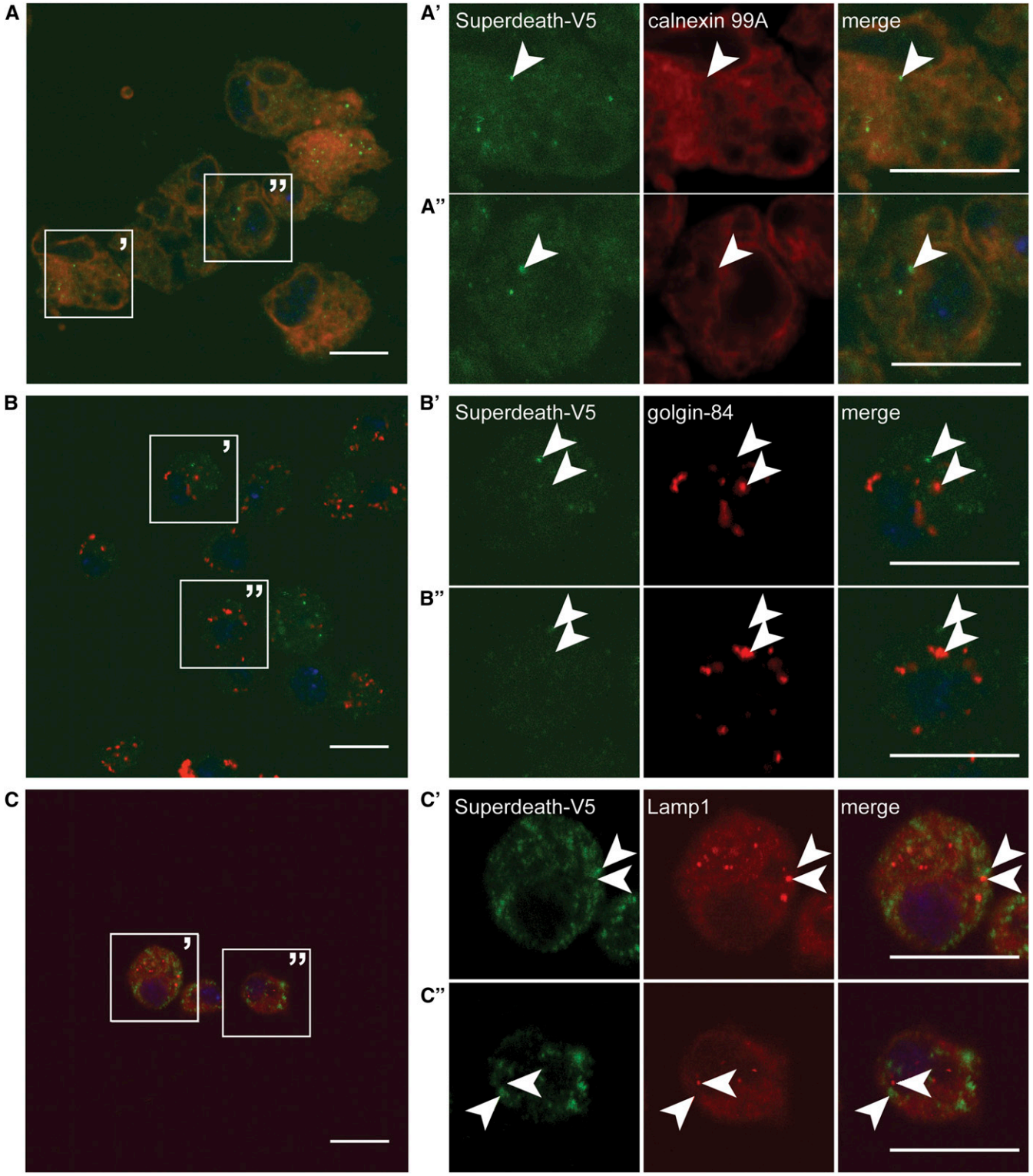

Figure 6 Superdeath is localized to the ER. Superdeath predominantly localizes to the ER membrane. (A) Superdeath localizes to the ER. S2 cells expressing Superdeath-V5 were stained for V5 (green) and Calnexin 99A (red) and counterstained with DAPI. A′ and A″ represent the highlighted panels from (A). White arrows highlight select sites of V5 and Calnexin 99A overlap. (B). Superdeath does not localize to the Golgi. S2 cells expressing Superdeath-V5 were stained for V5 (green) and Golgin-84 (red) and counterstained with DAPI. B′ and B″ represent the highlighted panels from (B). White arrows indicate select sites of independent V5 staining or Golgin-84 staining. (C). Superdeath does not primarily localize to the lysosome. S2 cells expressing Superdeath-V5 were stained for V5 (green) and Lamp1 (red) and counterstained with DAPI. C′ and C″ represent the highlighted panels from (C). White arrows indicate select sites of independent V5 staining or Lamp1 staining. Bar = 0.01 mm.

that, whereas Superdeath appears to colocalize with Calnexin 99A (Figure 6A), it does not colocalize with Golgin-84 (Figure 6B). Whereas the vast majority of the Superdeath and Lamp1 signals are distinct and nonoverlapping, we do detect a small minority of overlapping signals (Figure 6C). Importantly, in all cases, Superdeath does not appear to localize to the plasma membrane, the primary location of several potential human orthologs such as ANPEP, ENPEP, and LVRN. The staining for V5 is not detectable in cells not expressing the *superdeath* transgene (Figure S3). We concluded that Superdeath localizes and functions primarily at the ER membrane.

To confirm this localization, we also performed immunofluorescence staining for Superdeath in the salivary glands of L3 larvae. Salivary gland cells are large and have an extensive ER network due to their secretory functions. They are an ideal tissue in which to identify the subcellular localization of Superdeath. As in S2 cells, we stained for Calnexin 99A, Golgin-84, and Lamp1 in the salivary glands of larvae carrying a GFP-tagged allele of Superdeath (Superdeath-GFP; #64447 BDSC). Superdeath colocalizes with Calnexin 99A, but not with Golgin-84 or Lamp1 (Figure S4), similar to the colocalization observed in S2 cells. This is detectable by the extensive overlap as indicated by orange signals when costained with Calnexin 99A (Figure S4A). The vast majority of signals from Golgin-84 (Figure S4B) and Lamp1 (Figure S4C) lie adjacent to Superdeath-GFP, producing distinct red and green signals. Again, we do detect some potential overlap, though this time between Superdeath and Golgin-84. This might be due to close associations between the Golgi and ER membranes, or it may reflect some leakage of Superdeath protein to the Golgi, where it is then recycled back to the ER. We conclude that Superdeath localization is primarily to the ER membrane, and is similar in different cell types.

Discussion

Activation of the ER stress response and the subsequent cell death is a major contributor to the pathogenesis of a number of human diseases. Degenerative diseases are commonly caused or complicated by the accumulation of misfolded proteins in the ER and by stress-induced cell death (Hartong *et al.* 2006; Hetz and Saxena 2017; Zhu *et al.* 2017; Kurtishi *et al.* 2018; Yamanaka and Nukina 2018). In order to treat these degenerative diseases, it is essential to specifically target stress-associated cell death without inhibiting the beneficial stress-induced pathways that restore homeostasis.

In this study, we examined the metallopeptidase *superdeath*, a modifier of $Rh1^{G69D}$-induced degeneration (Chow *et al.* 2016). Loss of *superdeath* activity reduces apoptosis and degeneration without impacting the activation of the ER stress sensors IRE1 and PERK. Both of these sensors, while capable of initiating apoptosis upon chronic activation, have important cell survival functions that are essential for returning the stressed cell to homeostasis (Sano and Reed 2013). Loss of *superdeath* leaves these beneficial functions largely intact, and, instead, reduces the activation of JNK signaling through CDK5 activation. In this manner, *superdeath* orthologs could serve as important therapeutic targets to tip the balance in favor of cell survival in degenerative diseases.

Additionally, *superdeath* fills an important gap in ER stress-associated cell death biology. While previous studies have shown that CDK5 is responsible for activating the JNK signaling cascade under ER stress (Kang *et al.* 2012), the mechanism of how the stress signal is communicated to the kinase is still unknown. Our data suggest that the ER-associated Superdeath, which is likely orthologous to ERAP1 or ERAP2 in humans, may serve as an important bridge between ER stress and CDK5. Importantly, the active site of Superdeath is predicted to be present on the cytoplasmic side of the ER, suggesting that changes in ER membrane conformation and ER luminal environment could alter Superdeath activity, directly or indirectly activating CDK5.

There is already evidence that ERAP2 could be playing an important role in autoimmune disorders such as Crohn's disease and inflammatory arthritis, as well as in the response to viral infection (Franke *et al.* 2010; Popa *et al.* 2016; Ye *et al.* 2018). The types of stress responses induced in these diseases, including ER, oxidative, and mechanical stresses, frequently activate cell death through the JNK signaling cascade. This raises the possibility that Superdeath and ERAP2 are regulating apoptosis in response to many cellular stresses, and that these roles are not limited to the induction of ER stress; this is an exciting avenue of future study.

Our findings suggest that the *Drosophila* gene *superdeath* regulates stress-induced apoptosis. We have demonstrated a role for this gene in known apoptotic pathways and have shown that its role lies downstream of the beneficial activation of the UPR. The position of *superdeath* in the cellular stress response makes its orthologs attractive candidates for therapeutic targeting for a variety of diseases associated with ER stress-induced degeneration. Understanding how modifiers of stress-induced apoptosis are functioning in the cell also increases our understanding of degenerative diseases and provides new avenues for personalized therapies.

Acknowledgments

We thank Drs. Julie Hollien, Aylin Rodan, Anthea Letsou, and Carl Thummel for use of equipment and sharing reagents. We thank Dr. D. Allan Drummond for tremendous insight on Twitter and the name *superdeath*. This research was supported by an National Institutes of Health/National Institute of General Medical Sciences (NIH/NIGMS) R35 award (1R35GM124780) and a Glenn Award from the Glenn Foundation for Medical Research

to C.Y.C. C.Y.C. was the Mario R. Capecchi Endowed Chair in Genetics. R.A.S.P. is supported by a National Institute of Diabetes and Digestive and Kidney Diseases (NIDDK) T32 fellowship (5T32DK110966).

Literature Cited

Alicka, M., and K. Marycz, 2018 The effect of chronic inflammation and oxidative and endoplasmic reticulum stress in the course of metabolic syndrome and its therapy. Stem Cells Int. 2018: 4274361. https://doi.org/10.1155/2018/4274361

Bilak, A., and T. T. Su, 2009 Regulation of Drosophila melanogaster pro-apoptotic gene hid. Apoptosis 14: 943–949. https://doi.org/10.1007/s10495-009-0374-2

de Castro, E., C. J. A. Sigrist, A. Gattiker, V. Bulliard, P. S. Langendijk-Genevaux *et al*., 2006 ScanProsite: detection of PROSITE signature matches and ProRule-associated functional and structural residues in proteins. Nucleic Acids Res. 34: W362–W365. https://doi.org/10.1093/nar/gkl124

Chow, C. Y., M. F. Wolfner, and A. G. Clark, 2013 Using natural variation in Drosophila to discover previously unknown endoplasmic reticulum stress genes. Proc. Natl. Acad. Sci. USA 110: 9013–9018. https://doi.org/10.1073/pnas.1307125110

Chow, C. Y., X. Wang, D. Riccardi, M. F. Wolfner, and A. G. Clark, 2015 The genetic architecture of the genome-wide transcriptional response to ER stress in the mouse. PLoS Genet. 11: e1004924. https://doi.org/10.1371/journal.pgen.1004924

Chow, C. Y., K. J. P. Kelsey, M. F. Wolfner, and A. G. Clark, 2016 Candidate genetic modifiers of retinitis pigmentosa identified by exploiting natural variation in Drosophila. Hum. Mol. Genet. 25: 651–659. https://doi.org/10.1093/hmg/ddv502

Cox, J. S., and P. Walter, 1996 A novel mechanism for regulating activity of a transcription factor that controls the unfolded protein response. Cell 87: 391–404. https://doi.org/10.1016/S0092-8674(00)81360-4

Dombroski, B. A., R. R. Nayak, K. G. Ewens, W. Ankener, V. G. Cheung *et al*., 2010 Gene expression and genetic variation in response to endoplasmic reticulum stress in human cells. Am. J. Hum. Genet. 86: 719–729. https://doi.org/10.1016/j.ajhg.2010.03.017

FlyBase Curators, 2017 Frequently used GAL4 table data. Available at: https://flybase.org/reports/FBrf0237128#reference_sub

Franke, A., D. P. B. McGovern, J. C. Barrett, K. Wang, G. L. Radford-Smith *et al*., 2010 Genome-wide meta-analysis increases to 71 the number of confirmed Crohn's disease susceptibility loci. Nat. Genet. 42: 1118–1125. https://doi.org/10.1038/ng.717

Gaudet, P., M. S. Livstone, S. E. Lewis, and P. Thomas, 2011 Phylogenetic-based propagation of functional annotations within the Gene Ontology. Brief. Bioinform. 12: 449–462. https://doi.org/10.1093/bib/bbr042

Goyal, L., K. McCall, J. Agapite, E. Hartwieg, and H. Steller, 2000 Induction of apoptosis by Drosophila reaper, hid and grim through inhibition of IAP function. EMBO J. 19: 589–597. https://doi.org/10.1093/emboj/19.4.589

Haroon, N., and R. D. Inman, 2010 Endoplasmic reticulum aminopeptidases: biology and pathogenic potential. Nat. Rev. Rheumatol. 6: 461–467. https://doi.org/10.1038/nrrheum.2010.85

Hartong, D. T., E. L. Berson, and T. P. Dryja, 2006 Retinitis pigmentosa. Lancet 368: 1795–1809. https://doi.org/10.1016/S0140-6736(06)69740-7

Hay, B. A., D. A. Wassarman, and G. M. Rubin, 1995 Drosophila homologs of baculovirus inhibitor of apoptosis proteins function to block cell death. Cell 83: 1253–1262. https://doi.org/10.1016/0092-8674(95)90150-7

Hetz, C., and S. Saxena, 2017 ER stress and the unfolded protein response in neurodegeneration. Nat. Rev. Neurol. 13: 477–491. https://doi.org/10.1038/nrneurol.2017.99

Hollien J., and J. S. Weissman, 2006 Decay of endoplasmic reticulum-localized mRNAs during the unfolded protein response. Science 313: 104–107. https://doi.org/10.1126/science.1129631

Hollien, J., J. H. Lin, H. Li, N. Stevens, P. Walter *et al*., 2009 Regulated Ire1-dependent decay of messenger RNAs in mammalian cells. J. Cell Biol. 186: 323–331. https://doi.org/10.1083/jcb.200903014

Huang, W., M. A. Carbone, M. M. Magwire, J. A. Peiffer, R. F. Lyman *et al*., 2015 Genetic basis of transcriptome diversity in Drosophila melanogaster. Proc. Natl. Acad. Sci. USA 112: E6010–E6019. https://doi.org/10.1073/pnas.1519159112

Huang, H.-W. W., X. Zeng, T. Rhim, D. Ron, and H. D. Ryoo, 2017 The requirement of IRE1 and XBP1 in resolving physiological stress during Drosophila development. J. Cell Sci. 130: 3040–3049. https://doi.org/10.1242/jcs.203612

Jämsä, E., M. Simonen, and M. Makarow, 1994 Selective retention of secretory proteins in the yeast endoplasmic reticulum by treatment of cells with a reducing agent. Yeast 10: 355–370. https://doi.org/10.1002/yea.320100308

Jin, S., S. Martinek, W. S. Joo, J. R. Wortman, N. Mirkovic *et al*., 2000 Identification and characterization of a p53 homologue in Drosophila melanogaster. Proc. Natl. Acad. Sci. USA 97: 7301–7306. https://doi.org/10.1073/pnas.97.13.7301

Kanda, H., and M. Miura, 2004 Regulatory roles of JNK in programmed cell death. J. Biochem. 136: 1–6. https://doi.org/10.1093/jb/mvh098

Kang, M. J., J. Chung, and H. D. Ryoo, 2012 CDK5 and MEKK1 mediate pro-apoptotic signalling following endoplasmic reticulum stress in an autosomal dominant retinitis pigmentosa model. Nat. Cell Biol. 14: 409–415. https://doi.org/10.1038/ncb2447

Kang, K., H. D. Ryoo, J. E. Park, J. H. Yoon, and M. J. Kang, 2015 A Drosophila reporter for the translational activation of ATF4 marks stressed cells during development. PLoS One 10: e0126795. https://doi.org/10.1371/journal.pone.0126795

Krogh, A., B. Larsson, G. von Heijne, and E. L. Sonnhammer, 2001 Predicting transmembrane protein topology with a Hidden Markov Model: Application to complete genomes. J. Mol. Biol. 305: 567–580. https://doi.org/10.1006/jmbi.2000.4315

Kuranaga, E., H. Kanuka, T. Igaki, K. Sawamoto, H. Ichijo *et al*., 2002 Reaper-mediated inhibition of DIAP1-induced DTRAF1 degradation results in activation of JNK in Drosophila. Nat. Cell Biol. 4: 705–710. https://doi.org/10.1038/ncb842

Kurtishi, A., B. Rosen, K. S. Patil, G. W. Alves, and S. G. Møller, 2018 Cellular proteostasis in neurodegeneration. Mol. Neurobiol. 56: 3676–3689. https://doi.org/10.1007/s12035–018–1334-z

Mackay, T. F. C., S. Richards, E. A. Stone, A. Barbadilla, J. F. Ayroles *et al*., 2012 The Drosophila melanogaster genetic reference panel. Nature 482: 173–178. https://doi.org/10.1038/nature10811

Mollereau, B., and D. Ma, 2014 The p53 control of apoptosis and proliferation: lessons from Drosophila. Apoptosis 19: 1421–1429. https://doi.org/10.1007/s10495-014-1035-7

Palu, R. A. S., and C. Y. Chow, 2018 Baldspot/ELOVL6 is a conserved modifier of disease and the ER stress response. PLoS Genet. 14: e1007557. https://doi.org/10.1371/journal.pgen.1007557

Popa, O. M., M. Cherciu, L. I. Cherciu, M. I. Dutescu, M. Bojinca *et al*., 2016 ERAP1 and ERAP2 gene variations influence the risk of psoriatic arthritis in Romanian population. Arch. Immunol. Ther. Exp. (Warsz.) 64: 123–129. https://doi.org/10.1007/s00005-016-0444-4

Ryoo, H. D., P. M. Domingos, M.-J. J. Kang, and H. Steller, 2007 Unfolded protein response in a Drosophila model for

retinal degeneration. EMBO J. 26: 242–252. https://doi.org/10.1038/sj.emboj.7601477

Ryoo, H. D., J. Li, and M. J. Kang, 2013 Drosophila XBP1 expression reporter marks cells under endoplasmic reticulum stress and with high protein secretory load. PLoS One 8: e75774. https://doi.org/10.1371/journal.pone.0075774

Samali, A., U. Fitzgerald, S. Deegan, and S. Gupta, 2010 Methods for monitoring endoplasmic reticulum stress and the unfolded protein response. Int. J. Cell Biol. 2010: 830307. https://doi.org/10.1155/2010/830307

Sano, R., and J. C. Reed, 2013 ER stress-induced cell death mechanisms. Biochim. Biophys. Acta 1833: 3460–3470. https://doi.org/10.1016/j.bbamcr.2013.06.028

Schröder, M., and R. J. Kaufman, 2005 The mammalian unfolded protein response. Annu. Rev. Biochem. 74: 739–789. https://doi.org/10.1146/annurev.biochem.73.011303.074134

Shlevkov, E., and G. Morata, 2012 A dp53/JNK-dependant feedback amplification loop is essential for the apoptotic response to stress in Drosophila. Cell Death Differ. 19: 451–460. https://doi.org/10.1038/cdd.2011.113

Sidrauski, C., and P. Walter, 1997 The transmembrane kinase Ire1p is a site-specific endonuclease that initiates mRNA splicing in the unfolded protein response. Cell 90: 1031–1039. https://doi.org/10.1016/S0092-8674(00)80369-4

Sone, M., X. Zeng, J. Larese, and H. D. Ryoo, 2013 A modified UPR stress sensing system reveals a novel tissue distribution of IRE1/XBP1 activity during normal Drosophila development. Cell Stress Chaperones 18: 307–319. https://doi.org/10.1007/s12192-012-0383-x

Yamanaka, T., and N. Nukina, 2018 ER dynamics and derangement in neurological diseases. Front. Neurosci. 12: 91. https://doi.org/10.3389/fnins.2018.00091

Ye, C. J., J. Chen, A.-C. Villani, R. E. Gate, M. Subramaniam *et al.*, 2018 Genetic analysis of isoform usage in the human anti-viral response reveals influenza-specific regulation of ERAP2 transcripts under balancing selection. Genome Res. 28: 1812–1825. https://doi.org/10.1101/gr.240390.118

Yilmaz, E., 2017 Endoplasmic reticulum stress and obesity. Adv. Exp. Med. Biol. 960: 261–276. https://doi.org/10.1007/978-3-319-48382-5_11

Zhai, Z., N. Ha, F. Papagiannouli, A. Hamacher-Brady, N. Brady *et al.*, 2012 Antagonistic Regulation of Apoptosis and Differentiation by the Cut Transcription Factor Represents a Tumor-Suppressing Mechanism in Drosophila. *PLoS Genet.* 8: e1002582. https://doi.org/10.1371/journal.pgen.1002582

Zhang, Y., C. Cui, and Z. C. Lai, 2016 The defender against apoptotic cell death 1 gene is required for tissue growth and efficient N-glycosylation in Drosophila melanogaster. Dev. Biol. 420: 186–195. https://doi.org/10.1016/j.ydbio.2016.09.021

Zhu, B., L. Jiang, T. Huang, Y. Zhao, T. Liu *et al.*, 2017 ER-associated degradation regulates Alzheimer's amyloid pathology and memory function by modulating γ-secretase activity. Nat. Commun. 8: 1472. https://doi.org/10.1038/s41467-017-01799-4

Communicating editor: H. Bellen